Environmental Science & Technology

Article

Cite This: Environ. Sci. Technol. XXXX, XXX, XXX−XXX

pubs.acs.org/est

Zinc Isotope Fractionation during Sorption onto Al Oxides: Atomic Level Understanding from EXAFS

Wenxian Gou,[†] Wei Li,*[,†] Junfeng Ji,[†] and Weiqiang Li*[,‡]

[†]Key Laboratory of Surficial Geochemistry, Ministry of Education, School of Earth Sciences and Engineering, Nanjing University, Nanjing 210023, China

[‡]State Key Laboratory for Mineral Deposits Research, School of Earth Sciences and Engineering, Nanjing University, Nanjing 210023, China

Supporting Information

ABSTRACT: Interactions between aqueous Zn and mineral surfaces can lead to notable Zn isotope fractionation that affects Zn source fingerprinting, which needs an atomic-level understanding. In this study, we demonstrate that Zn isotope fractionation ($\Delta^{66}Zn_{sorbed\text{-}aqueous}$) during Zn sorption onto γ-Al_2O_3 depends on both pH and Zn concentration and ultimately correlates to surface coverage (Γ). At pH values of 6.0−6.5 and/or Zn concentrations of 0.1−0.2 mM, where Γ < 0.8 μmol m^{-2}, $\Delta^{66}Zn_{sorbed\text{-}solution}$ is 0.47 ± 0.03‰, whereas $\Delta^{66}Zn_{sorbed\text{-}aqueous}$ decreases to 0.02 ± 0.07‰ at pH values of 7.0−8.0 and Zn concentrations of 0.4−0.8 mM, with a high Γ ranging from 1.5 to 3.2 μmol m^{-2}. Using extended X-ray absorption fine structure (EXAFS) spectroscopy, we elucidated that a Zn−Al layered double hydroxide (LDH) with a Zn−O bond length of 2.06 Å forms at high surface coverage (1.5 < Γ < 3.2 μmol m^{-2}). In contrast, at low surface coverage (Γ < 0.8 μmol m^{-2}), the sorbed Zn occurs as a tetrahedrally coordinated inner-sphere surface complex with an average Zn−O interatomic distance of 1.98 Å. Such contrasts lead to an atomic level understanding of the strong links between isotope fractionation, local bonding structures (i.e., coordination and bond distances), and solution chemistry, which is crucial for more effective applications of stable metal isotopes as environmental tracers.

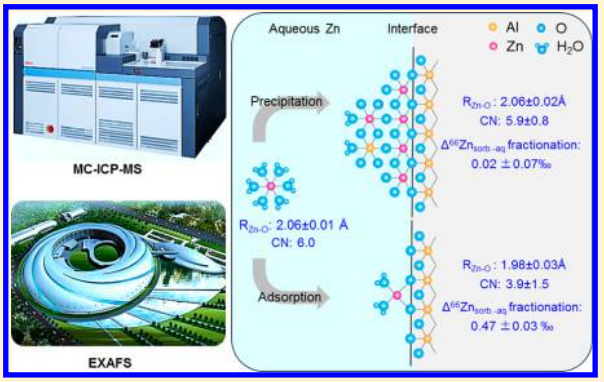

INTRODUCTION

Zinc is a first row transition metal that is ubiquitous in soils and aquatic environments. For living organisms, Zn is a micronutrient for organisms' growth and reproduction at background levels,[1,2] but it becomes toxic at elevated levels (>351 mg kg^{-1})[3] resulting from contaminations from human activities including agriculture, metallurgy, energy production, microelectronics, sewage sludge, and scrap disposal.[4,5] A fundamental understanding of the biogeochemical cycling of Zn in rivers, soils, and sediments affected by human activity is of significant importance for prediction of its environmental risks.

With the advances in high precision measurement of Zn isotopic ratios using multicollector inductively coupled-plasma mass spectrometry (MC-ICP-MS),[6] the Zn isotope system has been employed to give new perspectives for understanding paleoenvironments,[7,8] biogeochemical processes,[9] and metabolism-associated diseases.[10] Recently, considerable attention has been paid to the applications of Zn isotopes to understand the source and fate of heavy metals in the environment.[11−19] For example, Chen et al.[18,19] analyzed Zn isotopes to distinguish the anthropogenic sources of Zn in the Seine River and quantified the Zn contributions from roof runoff, roadway, and plant-treated and wastewater based on δ^{66}Zn signatures. In a different study, Juillot et al.[15] observed an upward trend of increasing δ^{66}Zn values in soils near a former Zn processing plant in northern France, where δ^{66}Zn increased from +0.22 ± 0.17‰ in the lower horizons to +0.76 ± 0.14‰ in the top soils. The high δ^{66}Zn values in top soils suggest the addition of franklinite-bearing slag, which has a heavy Zn isotope signature (+0.81 ± 0.20‰ in δ^{66}Zn).

Although case studies have demonstrated the great potential of Zn isotopes in fingerprinting environmental pollution,[11−19] challenges remain in application of the Zn isotope tracer even if the pollutant sources have distinctive isotopic signatures. This is because Zn isotope signatures from sources can be obscured by Zn isotope fractionation in geochemical processes such as precipitation-dissolution, incorporation, and sorption−desorption at mineral-aqueous solution interfaces.[20−28] Pokrovsky et al. (2005)[23] pioneered in investigating Zn isotope fractionation during sorption onto metal oxides. They found

Received: March 15, 2018
Revised: July 12, 2018
Accepted: July 15, 2018
Published: July 16, 2018

DOI: 10.1021/acs.est.8b01414
Environ. Sci. Technol. XXXX, XXX, XXX−XXX

that the surfaces of hematite, pyrolusite, gibbsite, and corundum tend to enrich heavy Zn isotopes, whereas goethite and birnessite surfaces enrich light Zn isotopes. Subsequently, more studies reported Zn isotope fractionation during interfacial sorption processes.[24−28] As summarized in Table S1, it is currently difficult to conclude a clear trend for Zn isotope fractionation behavior during sorption on mineral surfaces. For instance, the reported Zn isotopic fractionation ($\Delta^{66}Zn_{solid\text{-}aqueous}$) for birnessite varies from +0.05 ± 0.08‰ to +3.0‰.[23,25] Obviously, an atomic-level understanding of the Zn isotope fractionation behavior during interfacial reactions is a prerequisite for widely applying Zn isotopes for tracing pollution.

The complexities in Zn isotope fractionation during sorption onto mineral surfaces likely stem from variations in the chemical environment of the sorbed Zn at atomic scales, as metals in aqueous solution can be sorbed onto mineral surfaces via fundamentally different mechanisms (i.e., inner-sphere surface complexation, outer-sphere surface complexation, precipitation, and incorporation).[20−22] Theories of isotope fractionation suggest that heavy isotopes are enriched in substances with stronger bonds (e.g., low coordination number and shorter bond length) at equilibrium.[29] Extended X-ray absorption fine structure (EXAFS) spectroscopy is a powerful technique that can provide the local structural information (i.e., coordination number, bond distance) of specific metals.[21,30,31] EXAFS has been employed to study the chemical environment of transition metals (e.g., Co, Ni, Zn) during sorption onto several minerals,[21,32−34] but its applications to understanding isotope fractionation are still limited.[24,28]

In this study, we systematically investigated Zn isotope fractionation during its sorption onto γ-alumina (γ-Al_2O_3) under various pH and Zn loading conditions and employed EXAFS to reveal the Zn sorption mechanism. We chose γ-alumina as the adsorbent because (i) γ-alumina has well-defined surface properties and has been extensively used as a model compound for studying the mechanisms of heavy metal/metalloid sorption on metal oxides,[21,22] and (ii) naturally occurring Al-(hydr)oxides and clays commonly contain Zn impurities that can interfere with the measurement of sorbed Zn isotopes, while the Zn content in γ-alumina is negligible (~1.4 ppm). The objective of this research is to combine isotopic analysis and EXAFS analysis to elucidate the relationship between Zn isotope fractionation behavior and bonding structures of sorbed Zn at a molecular scale, which may ultimately help understand the transport and fate of Zn in the environment.

EXPERIMENTAL SECTION

Materials. Aluminum oxide (CAS: 1344-28-1) was purchased from Sigma-Aldrich as the adsorbent. Powder X-ray diffraction (XRD) analysis confirmed that this material was a pure γ-phase Al_2O_3 (Figure S1). The specific surface area of the powder was 106 ± 4 (2SD, n = 5) $m^2\ g^{-1}$, as measured by the multipoint (e.g., 8 points) N_2 Brunauer-Emmet-Teller method (BET). The Zn stock solution (40 mM, pH ≈ 3.4) used in this study was prepared from $Zn(NO_3)_2{\cdot}6H_2O$ (CAS: 10196-18-6, Sigma-Aldrich) and deionized water (>18.2 MΩ); all acids were purified by double sub-boiling distillation, and all labware involved in the experiments was made of Teflon to minimize Zn contamination.

Sorption Experiments. Three types of Zn sorption experiments were carried out under ambient conditions, including kinetic sorption experiments (duration of 0.5−48 h), sorption edge experiments (pH 4.0−9.0), and sorption isotherm experiments (Zn initial concentration of 0.1−0.8 mM). Prior to reacting with Zn in each sorption experiment, the γ-Al_2O_3 powder was hydrated in a 0.1 or 0.01 M $NaNO_3$ background electrolyte solution for 24 h at a fixed pH (4.0 to 9.0). After hydration, a certain amount of Zn stock solution was dispensed at a rate of approximately 1 mL min^{-1} while vigorously stirring the solution to avoid the formation of Zn precipitates due to local oversaturation of the suspension. The suspension was controlled at a solid/liquid ratio of 2.5 g L^{-1}, and the pH of the suspension was then maintained by titration with 0.01 M $NaOH/HNO_3$. After a reaction time of 0.5 to 48 h, the suspensions were centrifuged to separate the solids and supernatants, and the latter were further filtered through a methacrylate butadiene styrene filtration assembly with a poly(ether sulfone) membrane and 0.22 μm pores (Sartorius, Germany). The Zn concentration of the supernatant was analyzed by inductively coupled plasma-optical emission spectroscopy (Thermo ICP 6000 series ICP-OES, using emission lines of 213.8 and 206.1 nm).

Measurement of Zn Isotopes by MC-ICP-MS. After batch sorption experiments, the solids were separated from the supernatant by centrifugation and dissolved in 15 M HNO_3 at 95 °C in a capped Teflon vial for 24 h to extract the sorbed Zn for isotope analysis. The amount of aqueous Zn remaining in the pore space of γ-Al_2O_3 powders after centrifugation was lower than 1‰ of the sorbed Zn, based on the estimation of the Na content extracted by this step and the Na/Zn ratio of the supernatant. Aliquots of the sorbed Zn and aqueous Zn in supernatant from the sorption experiments were evaporated until dry and redissolved twice in 11 M HCl to convert Zn to a chloride form. After that, the samples were dissolved in 2 M HCl and prepared for ion exchange purification. The purified Zn was then separated from matrix elements following an anion exchange protocol modified from Maréchal et al.[6] (method details are provided in Table S2). Recovery of Zn for each sample was measured using ICP-OES and was confirmed to be quantitative (100 ± 6%). Total procedural blanks of Zn were monitored for each experimental run and were found to range from 4 to 24 ng (n = 12), which was negligible (<0.2%) compared with the ~10 μg Zn in each analyzed sample. After purification, the samples were dissolved in 0.05 M HNO_3 for isotopic analysis.

Zn isotope ratio measurement was performed using a Neptune Plus (Thermo Fisher Scientific) MC-ICP-MS at Nanjing University, China. The instrument was running at "wet-plasma" mode at low mass resolution ($M/\Delta M$ = 400), using a 120 μL min^{-1} self-aspirating nebulizer tip and a glass spray chamber. Instrument sensitivity was 10−14 V/ppm for ^{64}Zn (Table S3). Mass bias and instrumental drift were corrected using a combined sample-standard bracketing (SSB) and empirical external normalization (EEN) method with a Cu NIST647 dopant. A 40 s on-peak acid blank was measured before each isotope ratio measurement, which consisted of 50 4 s integrations. The typical internal precision (2 standard error or 2SE) was less than ±0.02‰ for $^{64}Zn/^{66}Zn$ or $^{65}Cu/^{63}Cu$.

The Zn isotopic compositions of all samples were reported relative to the IRMM 3702 standard as

DOI: 10.1021/acs.est.8b01414
Environ. Sci. Technol. XXXX, XXX, XXX−XXX

$$\delta^{66}\mathrm{Zn} = \left(\frac{\left(\frac{^{66}\mathrm{Zn}}{^{64}\mathrm{Zn}}\right)_{\mathrm{sample}}}{\left(\frac{^{66}\mathrm{Zn}}{^{64}\mathrm{Zn}}\right)_{\mathrm{IRMM\ 3702}}} - 1 \right) \times 1000 \quad (1)$$

Because all Zn isotope ratios are mass dependent (Figure S2), only δ^{66}Zn was reported in this study. The main matrix elements, Al and Na, do not affect the accuracy of Zn isotope measurements (Figure S3). The long-term external reproducibility of the $^{66/64}$Zn ratio measurement by MC-ICP-MS was better than 0.04‰ (2SD) based on repeat analysis of a standard solution over a period of 15 months (Figure S4). The measured δ^{66}Zn values of three reference materials (i.e., BCR, BHVO-2, AGV-2) are consistent with those reported in the literature (Table S4), attesting to the accuracy of the analytical procedure. The isotopic fractionation of Zn ($\Delta^{66}\mathrm{Zn}_{\mathrm{sorbed\text{-}aqueous}}$) between sorbed phase and aqueous phase is defined as

$$\Delta^{66}\mathrm{Zn}_{\mathrm{sorbed\text{-}aqueous}} = \delta^{66}\mathrm{Zn}_{\mathrm{sorbed}} - \delta^{66}\mathrm{Zn}_{\mathrm{aqueous}} \quad (2)$$

The error ($\mathrm{Error}\Delta^{66}\mathrm{Zn}_{\mathrm{sorbed\text{-}aqueous}}$) of Zn isotopic fractionation was calculated by the error propagation function:

$$\mathrm{Error}\Delta^{66}\mathrm{Zn}_{\mathrm{sorbed\text{-}aqueous}} = \sqrt{\mathrm{Error}\delta^{66}\mathrm{Zn}_{\mathrm{sorbed}}{}^{2} + \mathrm{Error}\delta^{66}\mathrm{Zn}_{\mathrm{aqueous}}{}^{2}} \quad (3)$$

$\mathrm{Error}\delta^{66}\mathrm{Zn}_{\mathrm{sorbed}}$ and $\mathrm{Error}\delta^{66}\mathrm{Zn}_{\mathrm{aqueous}}$ refer to the 2SD of $\delta^{66}\mathrm{Zn}_{\mathrm{sorbed}}$ and $\delta^{66}\mathrm{Zn}_{\mathrm{aqueous}}$, respectively.

EXAFS Data Collection and Analysis. The EXAFS spectroscopy of Zn *K*-edge was collected at room temperature on beamline 1W2B at Beijing Synchrotron Radiation Facility (BSRF). The electron storage ring operated at 2.5 GeV with an average current of 250 mA. A pair of Si(111) crystals was employed as the monochromator, which were detuned by 30% to suppress high-order harmonic contributions. Two reference standards, Zn−Al layered double hydroxide (LDH)[35] and Zn solution, were prepared as described in previous literature.[20,21] All sorption samples were placed at 45° to the incident beam so that EXAFS data could be recorded in both transmission mode and fluorescence mode.

EXAFS data analysis was performed using an IFEFFIT 1.2.11 program package.[36] The $\chi(k)$ function was Fourier transformed using k^3 weighting, and all shell-by-shell fitting was done in R-space to obtain the detailed local structural information. The theoretical scattering path was calculated based on the crystal structure of nikischerite[37] [Na-$Fe^{2+}{}_6Al_3(SO_4)_2(OH)_{18}(H_2O)_{12}$] by replacing Fe and Na with Zn. A single threshold energy value (ΔE_0) was allowed to vary during fitting. The amplitude reduction factor ($S_0{}^2$) was estimated to be 0.85 based on the fitting of $Zn(NO_3)_2$ solution and was then applied to sorption samples.

RESULTS AND DISCUSSION

Macroscopic Sorption Behaviors of Zn Sorption onto Al Oxide. Figure 1a illustrates the sorption behaviors of Zn on γ-Al_2O_3 as a function of the reaction time for experiments with initial Zn concentrations of 0.2 and 0.8 mM. The Zn sorption increased quickly over time and remained almost constant from 20 to 48 h. After 48 h of the reaction, approximately 97% of total Zn was removed from the solution in the 0.8 mM experiment, resulting in a surface coverage of 3.1 μmol m^{-2}. A surface coverage of 0.7 μmol m^{-2} was obtained from the 0.2 mM experiment based on its 93% Zn sorption. Based on these results, the reaction time for following sorption experiments was set to 48 h. Figure 1b reveals that the Zn sorption increased with both increasing pH and Zn concentration, consistent with previous studies.[21,22] At any given Zn concentration, the evolution of the sorption edge was characteristic of Zn sorption on Al-bearing (hydr)oxides and silicate,[20,26] with little sorption occurring below pH 6.0 but nearly 100% sorption occurring over a narrow pH range of 6.0−8.0. At any given pH value, the Zn sorption increased with increasing Zn initial concentration. Figure 1c shows that Zn sorption appears to be insensitive to ionic strength at pH 4−9,

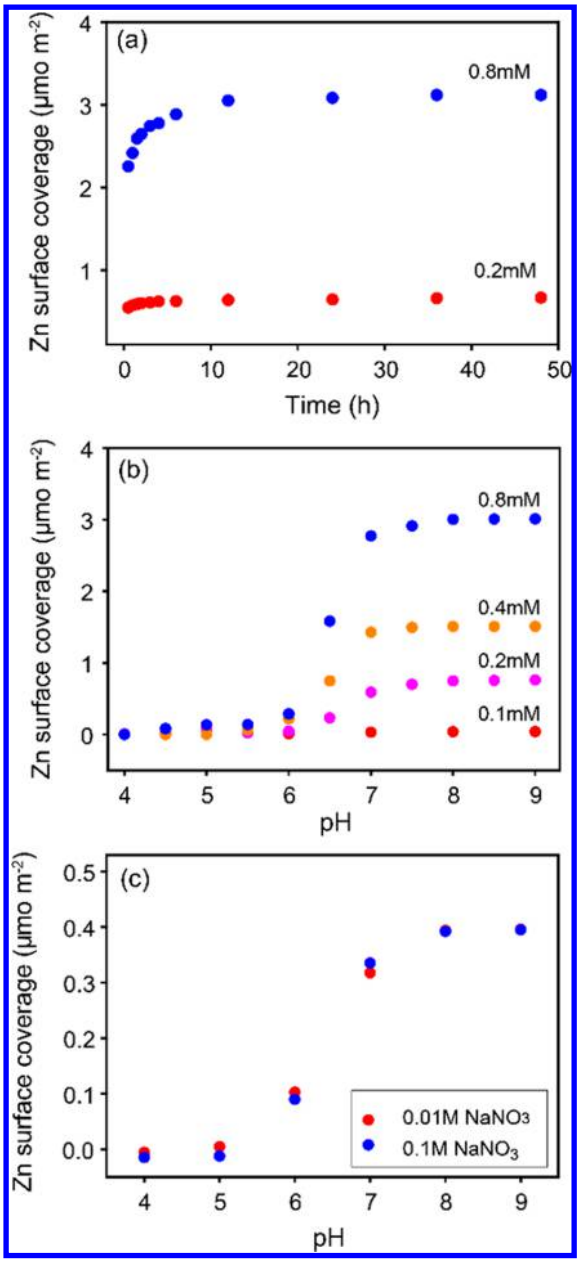

Figure 1. Macroscopic sorption behavior of Zn on γ-Al_2O_3. (a) Kinetics of Zn sorption on γ-Al_2O_3 at pH 7.5 in solutions of different Zn concentrations. Experiments were conducted in a 0.1 M $NaNO_3$ solution using a solid/solution ratio of 2.5 g/L; (b) Zinc sorption edges in solutions that have a constant ionic strength (0.1 M $NaNO_3$) but different initial Zn concentrations; (c): Zinc sorption edges in solutions that have the same initial Zn concentration (0.1 mM) but different ionic strengths (0.1 and 0.01 M $NaNO_3$).

DOI: 10.1021/acs.est.8b01414
Environ. Sci. Technol. XXXX, XXX, XXX−XXX

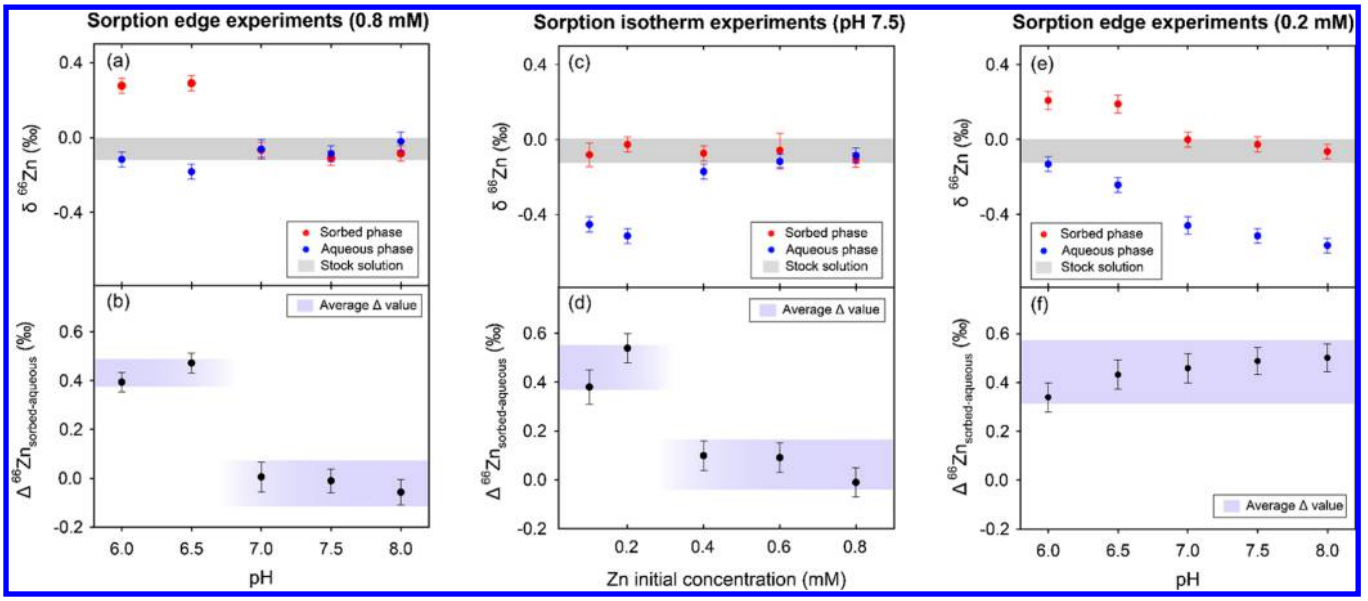

Figure 2. Plots of Zn isotope compositions of sorbed Zn and aqueous Zn and Zn isotopic fractionation between the two phases in sorption isotherm experiments (a, b), sorption edge experiments at 0.8 mM (c, d), and sorption edge experiments at 0.2 mM (e, f). The data in the figure correspond to those in Table S5.

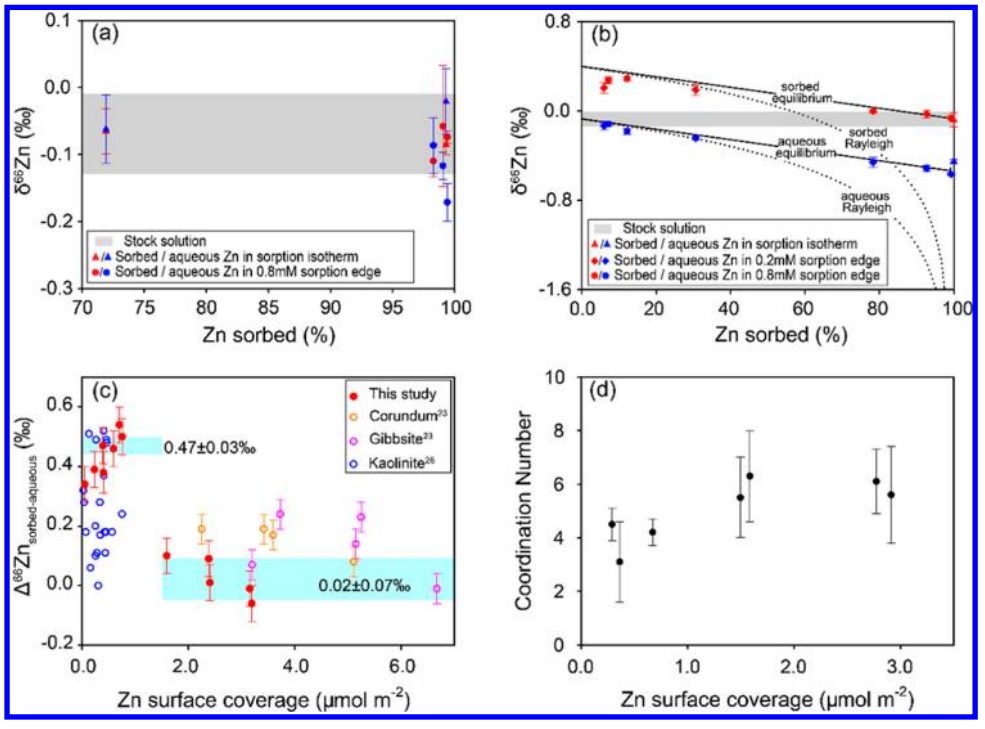

Figure 3. Plots of δ^{66}Zn values of sorbed Zn and aqueous Zn as a function of the fraction of sorbed Zn in experiments that have $\Gamma \leq 0.75$ μmol m^{-2} (a) and in experiments that have $\Gamma \geq 1.59$ μmol m^{-2} (b). The solid and dashed lines in the part b plot represent δ^{66}Zn values for sorbed Zn and aqueous Zn in the batch equilibrium model and the Rayleigh fractionation model, respectively. An isotopic fractionation factor, $\alpha^{66}Zn_{sorbed\text{-}aqueous}$, of 1.0047 ± 0.00003 is obtained based on the best-fit batch equilibrium model. (c) A summary of Zn isotope fractionation during Zn sorption onto the Al-rich mineral surface. The two cyan shades represent the average $\Delta^{66}Zn_{sorbed\text{-}aqueous}$ values for inner-sphere complexes and Zn−Al LDH precipitates in this study, respectively. (d) A plot of coordination number obtained from EXAFS data versus Zn surface coverage (Γ).

which excludes the formation of outer-sphere surface complexes, as previous experiments of Zn sorption on kaolinite and quartz at low pH conditions (3−5.5) have shown that the outer-sphere complexes are ionic-strength dependent.[26,28]

Behaviors of Zn Isotope Fractionation during Sorption onto γ-Al_2O_3. *Sorption Edge Experiments (0.8 mM).* Multiple experiments were conducted at different pH levels but with the same initial Zn concentration of 0.8 mM, and the results are presented in Figure 2a and Table S5. Based on the Zn isotope fractionation behavior, the experiments can be divided into two pH groups. In the pH 6.0−6.5 experiments, heavy Zn isotopes were preferentially partitioned onto the γ-Al_2O_3 surface relative to the aqueous Zn. Since the sorbed Zn accounted for a small fraction (<12%) of the initial

DOI: 10.1021/acs.est.8b01414
Environ. Sci. Technol. XXXX, XXX, XXX−XXX

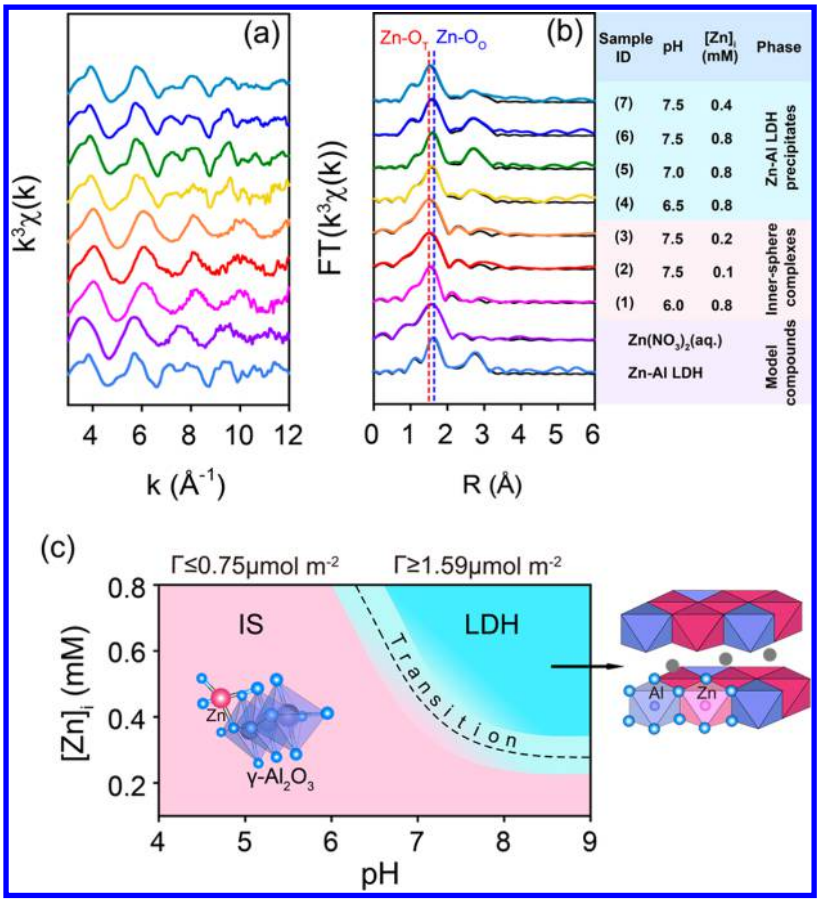

Figure 4. Zn *K*-edge EXAFS spectra of Zn-sorbed samples and model compounds as shown in Table 1: (a) k^3 weighted functions and (b) the corresponding Fourier transform without phase shift correction. The experimental data are shown as colored solid lines, and the fitted data are shown as black solid lines. (c) Schematic diagram showing the relationship between Zn sorption mechanism and pH and initial Zn concentration ($[Zn]_i$). Dashed curves and shaded regions are assigned based on EXAFS spectroscopic analyses of different experimental products. "IS" refers to inner-sphere complexes. "LDH" refers to "layered double hydroxide"

Zn in aqueous solution, the δ^{66}Zn values of the aqueous phase changed little after the sorption experiments due to isotope mass balance. In the pH 7.0−8.0 experiments, the δ^{66}Zn values of sorbed Zn and aqueous Zn overlapped within the analytical error and remained constant around −0.06 ± 0.06‰ (2SD, n = 6), the δ^{66}Zn value of the Zn stock solution. Zn isotope fractionation factors ($\Delta^{66}Zn_{sorbed\text{-}aqueous}$) were calculated to be +0.39 ± 0.06‰ to +0.47 ± 0.03‰ in the pH 6.0−6.5 experiments, in contrast to the close-to-zero fractionation (−0.06 ± 0.06‰ to 0.01 ± 0.06‰) in the pH 7.0−8.0 experiments (Figure 2b). It should be highlighted that the δ^{66}Zn and mass of the sorbed Zn and aqueous Zn satisfy isotope mass balance and that the calculated δ^{66}Zn for total Zn after sorption experiments is identical with the δ^{66}Zn of Zn stock solution (Table S5).

Sorption Isotherm Experiments (pH 7.5). The Zn isotope fractionation behavior was investigated in sorption isotherm experiments at a constant pH of 7.5 (Figure 2c and d). Similar to the 0.8 mM sorption edge experiments, heavy isotopes were enriched in the sorbed phase relative to the aqueous solution for experiments with initial Zn concentration of 0.1−0.2 mM, but there was no distinguishable Zn isotope fractionation in experiments with initial Zn concentrations of 0.4−0.8 mM (Figure 2c). Because the majority (>93%) of the initial Zn was sorbed onto the γ-Al_2O_3 surface, due to the isotope mass balance control, the sorption phase had δ^{66}Zn values similar to that of the Zn stock solution (−0.06 ± 0.06‰), but the Zn remaining in aqueous solution became isotopically light after sorption. This situation was opposite to that of the sorption edge experiments at 0.8 mM (Figure 2a). Nonetheless, the measured Zn isotope fractionations show a pattern similar to the 0.8 M sorption edge experiments: $\Delta^{66}Zn_{sorbed\text{-}aqueous}$ values decrease abruptly from +0.38 ± 0.07‰ ∼ +0.54 ± 0.06‰ to +0.10 ± 0.06‰ ∼ −0.01 ± 0.06‰ as the initial Zn concentration increases from 0.1−0.2 mM to 0.4−0.8 mM (Figure 2d).

Sorption Edge Experiments (0.2 mM). A third set of experiments investigated Zn sorption under variable pH values with a low initial Zn concentration of 0.2 mM. As shown in Figure 2e and Table S5, the results are different from the sorption edge experiments with an initial Zn concentration of 0.8 mM (Figure 2a) and consistently display the enrichment of Zn heavy isotopes onto the γ-Al_2O_3 surface relative to aqueous solution. As pH increased, $\delta^{66}Zn_{sorbed}$ evolved from +0.21 ± 0.05‰ at pH 6.0 toward −0.06 ± 0.04‰ at pH 8.0, which is close to that of the Zn stock solution, reflecting isotope mass balance with increasing Zn adsorption (Table S5). The $\delta^{66}Zn_{aqueous}$ value decreased correspondingly from −0.13 ± 0.04‰ at pH 6.0 to −0.57 ± 0.04‰ at pH 8.0, resulting in a relatively constant $\Delta^{66}Zn_{sorbed\text{-}aqueous}$ fractionation factor of 0.34 ± 0.06‰ to 0.50 ± 0.06‰ (Figure 2f).

DOI: 10.1021/acs.est.8b01414
Environ. Sci. Technol. XXXX, XXX, XXX−XXX

Table 1. Fitting Results of EXAFS Spectrum for Model Compounds and Sorption Samples (S_0^2 = 0.85)[b,c]

sample	R-factor	N_{idp}	N_{var}	χ^2	χ_v^2	shell no.	path	CN	R (Å)	σ^2 (Å^2)	ΔE (eV)	$\pm\sigma^2$ (Å^2)	$\pm\Delta E$ (eV)
$Zn(NO_3)_2$ aq	0.0002	10.8	10	35	54	1	Zn−O	6[a]	2.06	0.007	2.78	0.007	1.4
Zn−Al LDH	0.0005	17.5	17	123	270	1	Zn−O	6.5	2.08	0.008	−0.90	0.004	4.5
						2	Zn−Zn	3.5	3.10	0.010		0.004	
						2	Zn−Al	2.4	3.09	0.010		0.004	
Zn_0.8 mM pH 6.0	0.0026	18.8	14	214	44	1	Zn−O	4.5	1.98	0.008	−0.53	0.002	2.8
						2	Zn−Al	0.9	2.98	0.010		0.015	
Zn_0.8 mM pH 6.5	0.0007	17.7	16	79	47	1	Zn−O	6.3	2.05	0.012	0.85	0.001	0.4
						2	Zn−Zn	3.3	3.08	0.009		0.040	
						2	Zn−Al	1.9	3.07	0.011		0.004	
Zn_0.8 mM pH 7.0	0.0006	20.0	18	532	264	1	Zn−O	6.1	2.06	0.009	−0.75	0.002	2.1
						2	Zn−Zn	3.9	3.08	0.008		0.052	
						2	Zn−Al	1.8	3.07	0.008		0.004	
Zn_0.8 mM pH 7.5	0.0005	18.8	18	188	227	1	Zn−O	5.6	2.08	0.009	1.70	0.003	2.9
						2	Zn−Zn	4.0	3.11	0.009		0.039	
						2	Zn−Al	1.8	3.10	0.008		0.006	
Zn_0.4 mM pH 7.5	0.0002	12.2	9	316	121	1	Zn−O	5.5	2.04	0.011	−1.72	0.002	2.0
						2	Zn−Zn	2.9	3.09	0.011		0.036	
						2	Zn−Al	1.6	3.08	0.008		0.005	
Zn_0.2 mM pH 7.5	0.0023	19.7	14	311	56	1	Zn−O	4.2	1.98	0.007	1.16	0.001	2.3
						2	Zn−Al	0.5	3.00	0.006		0.013	
Zn_0.1 mM pH 7.5	0.0011	13.3	12	63	79	1	Zn−O	3.1	1.97	0.011	0.52	0.006	4.42
						2	Zn−Al	0.1	2.96	0.012		0.033	

[a]Fixed value. [b]S_0^2 is the amplitude reduction factor, estimated by the fitting for $Zn(NO_3)_2$ aq, and set to 0.85 for all samples; R-factor is the absolute misfit between experimental data and theory; N_{idp} is the number of independent points; N_{var} is the number of variables; χ^2 is the chi-square value; χ_v^2 is the reduced chi-square value; CN is the coordination number; R is the interatomic distance in Å; σ^2 in Å^2 is the Debye−Waller factor in Å^2; ΔE is the energy shift in eV. Estimated errors of bond distance is ± 0.01 Å for the first shell and ± 0.04 Å for the second shell. [c]Estimated errors for the first shell are ±20% for coordination numbers, and for second shell they are ±40% for coordination numbers.

Constraining Zn Isotope Fractionation Factors. In sorption experiments at pH values of 7.0−8.0 and Zn concentrations of 0.4−0.8 mM, the majority (74.9 to 99.9%) of aqueous Zn was sorbed as surface precipitates, and the $\delta^{66}Zn_{sorbed}$ values overlapped with the $\delta^{66}Zn_{aqueous}$ values as well as the $\delta^{66}Zn_{initial}$ value (Figure 3a). In these experiments, the Zn surface coverage was greater than 1.5 μmol m^{-2}, and the isotopic fractionation of Zn between the sorbed phase and the aqueous phase remained constant at $\Delta^{66}Zn_{sorbed\text{-}aqueous}$ = 0.02 ± 0.07‰. The lack of correlation between the fractionation factor and the degree of sorption (Figure 3a) implies isotopic equilibrium, which is in agreement with previous studies that suggested attainment of equilibrium Zn isotope fractionation within a few hours (e.g., <3 h) during Zn sorption onto the mineral surfaces of calcite,[27] quartz,[28] and amorphous silica.[28] Julliot et al. (2008)[24] also found that isotopic equilibrium had been reached within the first 16 h during Zn sorption onto 2-line ferrihydrite.

In contrast, in sorption experiments under slightly acidic (pH 6.0−6.5) conditions or with initial Zn concentration of 0.1−0.2 mM, where the Zn surface coverage was less than 0.8 μmol m^{-2}, a significant isotope fractionation occurred between the sorbed Zn and aqueous Zn, with $\Delta^{66}Zn_{sorbed\text{-}aqueous}$ ranging between 0.34 ± 0.06‰ and 0.54 ± 0.06‰. In these experiments, both $\delta^{66}Zn_{aqueous}$ and $\delta^{66}Zn_{sorbed}$ decreased with increasing proportion of sorbed Zn, plotting along two parallel trends in a diagram of $\delta^{66}Zn$ vs sorbed Zn fraction (Figure 3b). The experimental data were fitted using two models: one is a batch equilibrium model that assumes adequate exchange between the sorbed Zn and aqueous Zn at any given time irrespective of the degree of sorption, and the other is a Rayleigh model that mimics the effective separation of Zn from aqueous solution to the solid phase during sorption event. The two models can be described using the following equations

$$\delta^{66}Zn_{aqueous} = \frac{\delta^{66}Zn_{stock} - 1000 \times f \times (\alpha_{sorbed\text{-}aqueous} - 1)}{1 - f + (f \times \alpha_{sorbed\text{-}aqueous})} \quad \text{(Equilibrium model)} \tag{4}$$

$$\delta^{66}Zn_{aqueous} = \frac{1000 + \delta^{66}Zn_{stock}}{(1-f)^{\alpha_{sorbed\text{-}aqueous}}} - 1000 \quad \text{(Rayleigh model)} \tag{5}$$

where f stands for the fraction of sorbed Zn, and $\alpha_{sorbed\text{-}aqueous}$ refers to the (instant) isotope fractionation factor between aqueous Zn and sorbed Zn. The measured $\delta^{66}Zn_{stock}$ (−0.06 ± 0.06‰) was used in regression process.

Figure 3b demonstrates that the batch equilibrium model fits the observed data considerably better than the Rayleigh model, which attests to adequate isotope exchange between the aqueous solution and the Al-oxide mineral surface throughout the sorption experiments. Regression yields a $\alpha_{sorbed\text{-}aqueous}$ factor of 1.00047 ± 0.00003. According to eq 6, the isotope fractionation between aqueous Zn and sorbed Zn ($\Delta^{66}Zn_{sorbed\text{-}aqueous}$) can be calculated from $\alpha_{sorbed\text{-}aqueous}$.

$$\Delta^{66}Zn_{sorbed\text{-}aqueous} \cong 1000 \times \ln \alpha_{sorbed\text{-}aqueous} \tag{6}$$

This calculation yields a $\Delta^{66}Zn_{sorbed\text{-}aqueous}$ value of 0.47 ± 0.03‰, which is consistent with the one (0.44 ± 0.07‰) averaged from the measured Δ values.

To summarize, experiments with high Zn surface coverage (>1.5 μmol m^{-2}) and low Zn surface coverage (<0.8 μmol m^{-2}) show distinct Zn isotope fractionation behaviors (Figure 3c and Table S5). These facts imply that the fractionation of Zn isotopes during sorption signifies different sorption behaviors for the two groups of experiments.

DOI: 10.1021/acs.est.8b01414
Environ. Sci. Technol. XXXX, XXX, XXX−XXX

Bonding Structures of Zn Sorption Products As Revealed from EXAFS Spectroscopy. Figure 4a shows the normalized, background subtracted and k^3-weighted EXAFS spectra of Zn sorbed on γ-Al_2O_3 at pH values of 6.0−6.5 and/or Zn initial concentrations of 0.1−0.2 mM. Surface coverage from these experiments are in the range of 0.2 to 0.8 μmol m^{-2}. The spectra of reference compounds such as $Zn(NO_3)_2$ solution and synthetic crystalline Zn−Al layered double hydroxide (LDH) are also shown for comparison. The EXAFS spectra (Figure 4b) of all Zn-sorbed samples and $Zn(NO_3)_2$ solution display only one notable shell at 1.5 Å in Fourier transformed spectra, obviously differing from the Zn−Al LDH, which exhibits a second peak at r of 2.4 Å. Additionally, the oscillations in k^3-weighted χ spectra of these Zn sorbed samples differ from those of the $Zn(NO_3)_2$ solution. These features suggest that the local structure of the sorbed Zn is different from that of aqueous $Zn(NO_3)_2$ and Zn−Al LDH, thus excluding the formation of both outer-sphere surface complexes and surface precipitates. Shell-by-shell fitting results of the EXAFS spectra in Table 1 reveal that aqueous Zn is octahedrally coordinated by six oxygen atoms with a bond length of ∼2.06 Å, whereas the sorbed Zn is tetrahedrally coordinated by four oxygen atoms with an average Zn−O distance of 1.98 Å and a second Zn−Al shell (CN = 1−1.5) of 2.98 Å. Details of shell-by-shell fitting are provided in the Supporting Information (Figures S5 and S6 and Table S6). Such results indicate a predominant bidentate mononuclear inner-sphere surface complexation.[22] In addition, the XANES features for these samples (Supporting Information, Figure S7) are distinct from those for the Zn−Al LDH and $Zn(NO_3)_2$ solution, suggesting a Zn−O tetrahedral coordination and corroborating the above EXAFS analyses.[22]

Different from the samples prepared at pH of 6.0−6.5 and/or Zn initial concentrations of 0.1−0.2 mM, the surface coverage of samples at 7.0−7.5 pH and Zn initial concentration of 0.4−0.8 mM are remarkably higher (1.5 to 3.2 μmol m^{-2}). The EXAFS spectra (Figure 4a) of these high surface coverage samples are nearly identical, with all of them being similar to the Zn−Al LDH standard spectrum, with a complicated "beat" pattern appearing between 7 and 8 $Å^{-1}$, which is characteristic of Me(II)−Al(III) LDHs.[38−40] In the corresponding Fourier transformed spectra, two major peaks appear at ∼1.6 and 2.4 Å. The best fit data for the first shell suggests octahedral coordination of Zn with an average Zn−O bond length of 2.04−2.08 Å. The second shells can be fitted with a combination of Zn−Zn and Zn−Al scattering paths at ∼3.08 Å. These structural parameters are in agreement with the structure of typical Zn−Al LDH, which exhibits a brucite-like layered structure (Figure 4c), where 1/3 of the Zn in edge-sharing Zn−O octahedron is substituted by Al, generating a positive structural layer charge that is neutralized by interlayer anions.

Relationship between Zn Isotope Fractionation and Zn Sorption Mechanism. The distinct Zn isotope fractionation behaviors at different surface coverages can be explained by the difference in sorption complex structures (i.e., formation of surface complexes vs LDH precipitates) as revealed by the EXAFS analysis. More interesting is the clear correlation between the bonding environments of the sorbed Zn and Zn isotope fractionation during sorption. EXAFS data reveals that the Zn that adsorbed to the Al oxide surface at pH of 6.0−6.5 and/or Zn concentrations of 0.1−0.2 mM occurs as an inner-sphere surface complex (Γ < 0.8 μmol m^{-2}), with shorter Zn−O bond length (1.97 ± 0.03 (2SD, n = 3) Å) and lower coordination numbers (CN) (i.e., ∼4) than the aqueous Zn (R_{Zn-O} = 2.06 Å and CN = 6) (Figures 3d and S8). This difference in bonding environment contributes to a $\Delta^{66}Zn_{sorbed\text{-}aqueous}$ fractionation of +0.47 ± 0.03‰ between the two phases. In contrast, at Zn concentrations of 0.4−0.8 mM and pH of 7.0−7.5, the precipitated Zn in the Zn−Al LDH phase is present as octahedron surrounded by 6 oxygen atoms with R_{Zn-O} of 2.06 ± 0.02 Å, similar to the first shell of aqueous Zn^{2+}, the dominant Zn speciation at these conditions (Figure S9). Accordingly, there is little Zn isotope fractionation between the solid and aqueous phases. Note that Zn fractionation for the 0.4 mM sample is slightly higher than that for the 0.6 and 0.8 mM samples, which may imply a presence of mixed Zn−Al LDH precipitates and a small amount of tetrahedral inner-sphere surface complexes, consistent with its relatively lower amplitude of second shell in its Fourier transformed EXAFS spectrum. Furthermore, our laboratory finding is in good agreement with the results from a previous field study. Aucour et al. (2015) demonstrated that soils containing octahedral Zn (Zn-LDH and sorbed species) are enriched in light isotopes, whereas the DTPA exchangeable tetrahedral Zn species are enriched in heavy isotopes.[41]

The fractionation factor of $\Delta^{66}Zn_{sorbed\text{-}aqueous}$ of 0.47 ± 0.03‰ appears to be consistent with those associated with sorption onto several different metal hydroxides. A recent study suggested that Zn sorption to the edge sites of kaolinite yields a $\Delta^{66}Zn_{sorbed\text{-}aqueous}$ fractionation of 0.49 ± 0.06‰.[26] This may not be surprising because of the similarity between the surface functional groups (>AlOH) of naturally occurring clays such as kaolinite and the reactive sites of the Al oxide surfaces in this study. However, a similar Zn isotope fractionation during adsorption has also been observed for other Al-free minerals. For example, sorption of Zn onto calcite results in a $\Delta^{66}Zn_{sorbed\text{-}aqueous}$ fractionation of 0.41 ± 0.18‰ at low ionic strength conditions.[27] Additionally, both Juillot et al. (2008)[24] and Balistrieri et al. (2008)[42] demonstrated that Zn sorption onto ferrihydrite led to a $\Delta^{66}Zn_{sorbed\text{-}aqueous}$ fractionation of approximately 0.52‰, where the sorbed Zn occurs as tetrahedral inner-sphere surface complexes. In addition to the experimental studies discussed above, the δ^{66}Zn of natural Fe−Mn crusts and nodules is ∼0.5‰ higher than the δ^{66}Zn of the deep seawater.[43] EXAFS analyses indicated that Zn fixed in the Fe−Mn crusts and nodules is surrounded by 4 oxygen atoms with bond lengths of ∼1.97 Å.[43] These similarities reveal a strong link between the speciation of Zn as tetrahedral inner-sphere surface complexes and the enrichment of heavy Zn isotopes.

The consistency in Zn isotope fractionation factors during sorption onto different mineral surfaces seems to imply that the coordination number for the first shell has the dominant isotopic effect over the nature of the secondary shells for the sorbed Zn on mineral surfaces. However, it should be emphasized that bond length and structural order also contribute significantly to the isotope fractionation of Zn during its sorption on metal oxides. As shown in Figure 5, it is clear that heavy Zn isotopes are favorably partitioned into phases with stronger bonds that have lower coordination number and shorter bond length.[29,44−46] Notably, the adsorption of Zn on SiO_2 surfaces results in the shortest Zn−O bond distance (1.93 ± 0.02 Å) that correlates to the greatest Zn isotope fractionation (0.8−1.2‰) noted in the literature. Overall, this is in accordance with classic theories of

DOI: 10.1021/acs.est.8b01414
Environ. Sci. Technol. XXXX, XXX, XXX−XXX

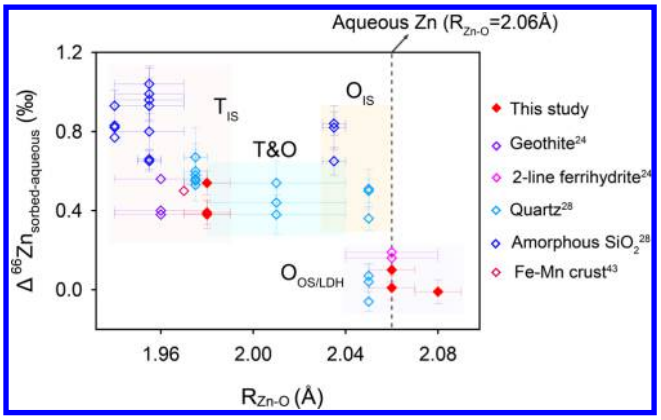

Figure 5. A summary plot of the correlation between Zn−O bond length as revealed by EXAFS spectroscopy and the Zn isotope fractionation factors during sorption to different minerals. T_{IS} (translucent red shading) refers to tetrahedral inner-sphere Zn complexation, O_{IS} (translucent orange shading) refers to octahedral inner-sphere Zn complexation, $O_{OS/LDH}$ (translucent cyan shading) refers to Zn−Al LDH and outer-sphere Zn complexation in octahedral coordination, and T&O (translucent pink shading) refers to a mixture of octahedral Zn complexes and tetrahedral Zn complexation. Note that the R_{Zn-O} for either quartz or amorphous SiO_2 was estimated from the correlation between surface coverage and EXAFS analysis.[28] The vertical and horizontal error bars represent uncertainty (2 standard deviation) in $\Delta^{66}Zn_{sorbed-aqueous}$ values and R_{Zn-O}, respectively.

isotope distribution that state that equilibrium isotope fractionation between different phases is predominantly correlated with vibrational energies,[44,45] which are controlled by the bond strength of the element of interest at the molecular scale. A more quantitative understanding of the relationship between bond distance and isotopic fractionation requires substantial spectroscopic data and theoretical modeling.[49−53]

Environmental Implications. This study shows that environmental conditions (i.e., physicochemical parameters such as pH and concentration) play an important role in controlling Zn sorption behavior, surface coverage, molecular scale bonding environments (e.g., Zn coordination and atomic bond distances), and Zn fractionation factors. In turn, this study establishes excellent correlations among those measurable parameters, meaning that signatures from Zn isotopes could be used as effective tracers in studies of the biogeochemical cycling and fate of Zn in Earth's surface environment. Specifically, we demonstrate that significant Zn fractionation occurs on the mineral/solution interface at $[Zn^{2+}]$ < 0.2 mM, suggesting the necessity of considering Zn fractionation behaviors in investigations of Zn transport in aqueous environments where the concentration of aqueous Zn is typically low. As the presence of organic ligands in soils and sediments can affect LDH formation and the structures of aqueous and surface complexes of metals, the possible isotopic effect of organic ligands[54] on Zn isotope fractionation should be taken into account in future studies.

Furthermore, our results shed light on the application of Zn isotopes for source apportionment.[11−19] A large variation of Zn isotope compositions has been measured from Zn-rich reservoirs, such as high temperature igneous rocks ($\delta^{66}Zn_{JMC}$ of ∼0.3‰),[1] Zn-rich ore minerals (∼0.11‰),[1] carbonates (0.91‰),[7] franklinite-bearing slag (∼0.81‰),[15] and air emission particles (−0.36‰).[47] Such a range of composition is significantly greater than that resulting from isotope variation induced by Zn sorption on Al oxide, Fe oxyhydroxide, and kaolinite surfaces (0.47−0.52 ‰). This implies that Zn isotopes are still effective for tracing polluting processes for target reservoirs exhibiting a Zn isotopic contrast that is large enough (>0.47‰, the fractionation value during sorption process) in highly weathered environments (e.g., tropical soils) where Fe/Al oxides and clays are abundant.[48]

■ ASSOCIATED CONTENT

Supporting Information

The Supporting Information is available free of charge on the ACS Publications website at DOI: 10.1021/acs.est.8b01414.

Summary of previous studies on Zn isotope fractionation during sorption onto minerals (Table S1); XRD analysis of aluminum oxide (Figure S1); ion-exchange purification of Zn (Table S2); mass spectrometry for Zn isotope analysis (Table S3); mass dependent behavior Zn isotope analysis (Figure S2); robustness of the analytical method for Zn isotopes (Figures S3 and S4); accuracy of Zn isotope analysis (Table S4); long-term external reproducibility of Zn isotope analysis (Figure S4); chemical and isotopic results of Zn sorption experiments (Table S5); shell-by-shell fitting for EXAFS spectra (Figures S5 and S6, Table S6); local structure of sorbed Zn obtained from XANES spectra (Figure S7); local structure of sorbed Zn versus surface density (Figure S8); speciation of aqueous Zn (Figure S9) (PDF)

■ AUTHOR INFORMATION

Corresponding Authors

*Phone: +(86 25) 89681539. E-mail: liwei_isg@nju.edu.cn (Wei Li).

*E-mail: liweiqiang@nju.edu.cn (Weiqiang Li).

ORCID

Wei Li: 0000-0002-0789-0320

Notes

The authors declare no competing financial interest.

■ ACKNOWLEDGMENTS

We sincerely appreciate the helpful comments from four anonymous reviewers and from our editor, Dr. Giammar. This research was supported by the National Natural Science Foundation of China (NSFC) (Grant Nos. 41473084, 41722303, 41571130061) and the Distinguished Young Scientists Program of Jiangsu Province (BK20150018). Both Wei Li and Weiqiang Li are grateful for the financial support of the Start-Up grants from Nanjing University, the 1000 Youth Talent Program sponsored by the Chinese central government, and the support from Chinese Academy of Sciences's State Key Laboratory of Environmental Chemistry and Ecotoxicology (KF2015-03) and Key Laboratory of Soil Environment and Pollution Remediation (SEPR2017-01). We acknowledge assistance from Prof. Gaojun Li, Mrs. Le Li, and Laifeng Li for MC-ICP-MS analysis. EXAFS data collection was mainly carried out with the assistance of Drs. Jing Zhang and Lirong Zheng at the 1W1B beamline of Beijing Synchrotron Radiation Facility (BSRS), and part of the EXAFS data was collected at the 14W beamline at Shanghai Synchrotron Radiation Facility (SSRF) operated by the Chinese Academy of Sciences.

DOI: 10.1021/acs.est.8b01414
Environ. Sci. Technol. XXXX, XXX, XXX−XXX

REFERENCES

(1) Moynier, F.; Vance, D.; Fujii, T.; Savage, P. The isotope geochemistry of zinc and copper. *Rev. Mineral. Geochem.* **2017**, *82*, 543−600.

(2) Morel, F. M. M.; Reinfelder, J. R.; Roberts, S. B.; Chamberlain, C. P.; Lee, J. G.; Yee, D. Zinc and carbon co-limitation of marine phytoplankton. *Nature* **1994**, *369*, 740−742.

(3) Jennings, A. A. Analysis of worldwide regulatory guidance values for the most commonly regulated elemental surface soil contamination. *J. Environ. Manage.* **2013**, *118*, 72−95.

(4) Adriano, D. C. *Trace Elements in the Terrestrial Environment*; Springer: New York, 2001; DOI: 10.1007/978-0-387-21510-5.

(5) Rout, G. R.; Das, P. Effect of metal toxicity on plant growth and metabolism:I. zinc. *Agronomie* **2003**, *23*, 3−11.

(6) Maréchal, C. N.; Télouk, P.; Albarède, F. Precise analysis of copper and zinc isotopic compositions by plasma-source mass spectrometry. *Chem. Geol.* **1999**, *156*, 251−273.

(7) Pichat, S.; Douchet, C.; Albarède, F. Zinc isotope variations in deep-sea carbonates from the eastern equatorial Pacific over the last 175 Ka. *Earth Planet. Sci. Lett.* **2003**, *210*, 167−178.

(8) Pons, M. L.; Fujii, T.; Rosing, M.; Quitté, G.; Télouk, P.; Albarède, F. A Zn isotope perspective on the rise of continents. *Geobiology* **2013**, *11*, 201−214.

(9) Maréchal, C. N.; Nicolas, E.; Douchet, C.; Albarède, F. Abundance of zinc isotopes as a marine biogeochemical tracer. *Geochem., Geophys., Geosyst.* **2000**, *1*, 1−15.

(10) Albarède, F.; Télouk, P.; Balter, V. Medical applications of isotope metallomics. *Rev. Mineral. Geochem.* **2017**, *82*, 851−885.

(11) Cloquet, C.; Carignan, J.; Libourel, G. Isotopic composition of Zn and Pb atmospheric depositions in an urban/Periurban area of northeastern France. *Environ. Sci. Technol.* **2006**, *40*, 6594−6600.

(12) Dolgopolova, A.; Weiss, D. J.; Seltmann, R.; Kober, B.; Mason, T. F. D.; Coles, B.; Stanley, C. J. Use of isotope ratios to assess sources of Pb and Zn dispersed in the environment during mining and ore processing within the Orlovka−Spokoinoe mining site (Russia). *Appl. Geochem.* **2006**, *21*, 563−579.

(13) John, S. G.; Park, J. G.; Zhang, Z.; Boyle, E. A. The isotopic composition of some common forms of anthropogenic zinc. *Chem. Geol.* **2007**, *245*, 61−69.

(14) Araújo, D. F.; Boaventura, G. R.; Machado, W.; Viers, J.; Weiss, D.; Patchineelam, S. R.; Ruiz, I.; Rodrigues, A. P. C.; Babinski, M.; Dantas, E. Tracing of anthropogenic zinc sources in coastal environments using stable isotope composition. *Chem. Geol.* **2017**, *449*, 226−235.

(15) Juillot, F.; Maréchal, C.; Morin, G.; Jouvin, D.; Cacaly, S.; Telouk, P.; Benedetti, M. F.; Ildefonse, P.; Sutton, S.; Guyot, F. Contrasting isotopic signatures between anthropogenic and geogenic Zn and evidence for post-depositional fractionation processes in smelter-impacted soils from Northern France. *Geochim. Cosmochim. Acta* **2011**, *75*, 2295−2308.

(16) Petit, J. C. J.; Schäfer, J.; Coynel, A.; Blanc, G.; Chiffoleau, J. F.; Auger, D.; Bossy, C.; Drriennic, H.; Mikolaczyk, M.; Dutruch, L. The estuarine geochemical reactivity of Zn isotopes and its relevance for the biomonitoring of anthropogenic Zn and Cd contaminations from metallurgical activities: example of the Gironde fluvial-estuarine system, France. *Geochim. Cosmochim. Acta* **2015**, *170*, 108−125.

(17) Weiss, D. J.; Rausch, N.; Mason, T. F. D.; Coles, B. J.; Wilkinson, J. J.; Ukonmaanaho, L.; Arnold, T.; Nieminen, T. M. Atmospheric deposition and isotope biogeochemistry of zinc in ombrotrophic peat. *Geochim. Cosmochim. Acta* **2007**, *71*, 3498−3517.

(18) Chen, J.; Gaillardet, J.; Louvat, P. Zinc isotopes in the Seine river waters, France: A probe of anthropogenic contamination. *Environ. Sci. Technol.* **2008**, *42*, 6494−6501.

(19) Chen, J. B.; Gaillardet, J.; Louvat, P.; Huon, S. Zn isotopes in the suspended load of the Seine river, France: isotopic variations and source determination. *Geochim. Cosmochim. Acta* **2009**, *73*, 4060−4076.

(20) Roberts, D. R.; Ford, R. G.; Sparks, D. L. Kinetics and mechanisms of Zn complexation on metal oxides using EXAFS spectroscopy. *J. Colloid Interface Sci.* **2003**, *263*, 364−376.

(21) Li, W.; Xu, W.; Livi, K. J. T.; Siebecker, M. G.; Wang, Y.; Phillips, B. L.; Sparks, D. L. Formation of crystalline Zn-Al layered double hydroxide precipitates on γ-alumina: The role of mineral dissolution. *Environ. Sci. Technol.* **2012**, *46*, 11670−11677.

(22) Trainor, T. P.; Brown, G. E.; Parks, G. A. Adsorption and precipitation of aqueous Zn (II) on alumina powders. *J. Colloid Interface Sci.* **2000**, *231*, 359−372.

(23) Pokrovsky, O. S.; Viers, J.; Freydier, R. Zinc stable isotope fractionation during its adsorption on oxides and hydroxides. *J. Colloid Interface Sci.* **2005**, *291*, 192−200.

(24) Juillot, F.; Maréchal, C.; Ponthieu, M.; Cacaly, S.; Morin, G.; Benedetti, M.; Hazemann, J. L.; Proux, O.; Guyot, F. Zn isotopic fractionation caused by sorption on goethite and 2-lines ferrihydrite. *Geochim. Cosmochim. Acta* **2008**, *72*, 4886−4900.

(25) Bryan, A. L.; Dong, S.; Wilkes, E. B.; Wasylenki, L. E. Zinc isotope fractionation during adsorption onto Mn oxyhydroxide at low and high ionic strength. *Geochim. Cosmochim. Acta* **2015**, *157*, 182−197.

(26) Guinoiseau, D.; Gélabert, A.; Moureau, J.; Louvat, P.; Benedetti, M. F. Zn isotope fractionation during sorption onto kaolinite. *Environ. Sci. Technol.* **2016**, *50*, 1844−1852.

(27) Dong, S.; Wasylenki, L. E. Zinc isotope fractionation during adsorption to calcite at high and low ionic strength. *Chem. Geol.* **2016**, *447*, 70−78.

(28) Nelson, J.; Wasylenki, L.; Bargar, J. R.; Brown, G. E.; Maher, K. Effects of surface disorder and surface coverage on isotopic fractionation during Zn(II) adsorption onto quartz and amorphous silica surfaces. *Geochim. Cosmochim. Acta* **2017**, *215*, 354−376.

(29) Schauble, E. A. Applying stable isotope fractionation theory to new systems. *Rev. Mineral. Geochem.* **2004**, *55*, 65−111.

(30) Sayers, D. E.; Stern, E. A.; Lytle, F. W. New technique for investigating noncrystalline structures: fourier analysis of the extended X-ray-absorption fine structure. *Phys. Rev. Lett.* **1971**, *27* (18), 1204−1207.

(31) Lombi, E.; Susini, J. Synchrotron-based techniques for plant and soil science: opportunities, challenges and future perspectives. *Plant Soil* **2009**, *320*, 1−35.

(32) Scheidegger, A. M.; Lamble, G. M.; Sparks, D. L. Investigation of Ni Sorption on Pyrophyllite: An XAFS Study. *Environ. Sci. Technol.* **1996**, *30*, 548−554.

(33) Catalano, J. G.; Warner, J. A.; Brown, G. E. Sorption and precipitation of Co(II) in Hanford sediments and alkaline aluminate solutions. *Appl. Geochem.* **2005**, *20*, 193−205.

(34) Toner, B.; Manceau, A.; Webb, S. M.; Sposito, G. Zinc sorption to biogenic hexagonal-birnessite particles within a hydrated bacterial biofilm. *Geochim. Cosmochim. Acta* **2006**, *70*, 27−43.

(35) Gou, W.; Siebecker, M. G.; Wang, Z.; Li, W. Competitive sorption of Ni and Zn at the aluminum oxide/water interface: an XAFS study. *Geochem. Trans.* **2018**, *19*, 9.

(36) Ravel, B.; Newville, M. ATHENA, ARTEMIS, HEPHAESTUS: data analysis for X-ray absorption spectroscopy using Ifeffit. *J. Synchrotron Radiat.* **2005**, *12*, 537−541.

(37) Huminicki, D. M. C.; Hawthorne, F. C. The crystal structure of nikischerite, $NaFe^{2+}{}_6Al_3(SO_4)_2(OH)_{18}(H_2O)_{12}$, a mineral of the shigaite group. *Can. Mineral.* **2003**, *41*, 79−82.

(38) Scheinost, A. C.; Sparks, D. L. Formation of layered single- and double-metal hydroxide precipitates at the mineral/water interface: a multiple-scattering XAFS analysis. *J. Colloid Interface Sci.* **2000**, *223*, 167−178.

(39) Thompson, H. A.; Parks, G. A.; Brown, G. E. Dynamic interactions of dissolution, surface adsorption, and precipitation in an aging cobalt(II)-clay-water system. *Geochim. Cosmochim. Acta* **1999**, *63*, 1767−1779.

(40) Towle, S. N.; Bargar, J. R.; Brown, G. E.; Parks, G. A. Surface precipitation of Co(II)(aq) on Al_2O_3. *J. Colloid Interface Sci.* **1997**, *187* (1), 62−82.

DOI: 10.1021/acs.est.8b01414
Environ. Sci. Technol. XXXX, XXX, XXX−XXX

(41) Aucour, A. M.; Bedell, J. P.; Queyron, M.; Magnin, V.; Testemale, D.; Sarret, G. Dynamics of Zn in an urban wetland soil-plant system: coupling isotopic and EXAFS approaches. *Geochim. Cosmochim. Acta* **2015**, *160*, 55−69.
(42) Balistrieri, L. S.; Borrok, D. M.; Wanty, R. B.; Ridley, W. I. Fractionation of Cu and Zn isotopes during adsorption onto amorphous Fe(III) oxyhydroxide: experimental mixing of acid rock drainage and ambient river water. *Geochim. Cosmochim. Acta* **2008**, *72* (2), 311−328.
(43) Little, S. H.; Sherman, D. M.; Vance, D.; Hein, J. R. Molecular controls on Cu and Zn isotopic fractionation in Fe−Mn crusts. *Earth Planet. Sci. Lett.* **2014**, *396* (12), 213−222.
(44) Urey, H. C. The thermodynamic properties of isotopic substances. *J. Chem. Soc.* **1947**, *1*, 562−581.
(45) Bigeleisen, J.; Mayer, M. G. Calculation of Equilibrium Constants for Isotopic Exchange Reactions. *J. Chem. Phys.* **1947**, *15* (5), 261−267.
(46) O'Neil, J. R. Theoretical and experimental aspects of isotopic fractionation. *Rev. Mineral. Geochem.* **1986**, *16*, 1−40.
(47) Yin, N. H.; Sivry, Y.; Benedetti, M. F.; Lens, P. N. L.; Hullebusch, E. D. V. Application of Zn isotopes in environmental impact assessment of Zn−Pb metallurgical industries: A mini review. *Appl. Geochem.* **2016**, *64* (4), 128−135.
(48) Araújo, D. F.; Boaventura, G. R.; Machado, W.; Viers, J.; Weiss, D.; Patchineelam, S. R.; Ruiz, I.; Rodrigues, A. P.; Babinski, D.; Dantas, E. Tracing of anthropogenic zinc sources in coastal environments using stable isotope composition. *Chem. Geol.* **2017**, *449*, 226−235.
(49) Barling, J.; Anbar, A. D. Molybdenum isotope fractionation during adsorption by manganese oxides. *Earth Planet. Sci. Lett.* **2004**, *217*, 315−329.
(50) Wasylenki, L. E.; Weeks, C. L.; Bargar, J. R.; Spiro, T. G.; Hein, J. R.; Anbar, A. D. The molecular mechanism of Mo isotope fractionation during adsorption to birnessite. *Geochim. Cosmochim. Acta* **2011**, *75*, 5019−5031.
(51) Brennecka, G. A.; Wasylenki, L. E.; Bargar, J. R.; Weyer, S.; Anbar, A. D. Uranium isotope fractionation during adsorption to Mn-oxyhydroxides. *Environ. Sci. Technol.* **2011**, *45*, 1370−1375.
(52) Ducher, M.; Blanchard, E.; Balan, E. Equilibrium isotopic fractionation between aqueous Zn and minerals from first-principles calculations. *Chem. Geol.* **2018**, *483*, 342−350.
(53) Veeramani, H.; Eagling, J.; Jamieson-Hanes, J. H.; Kong, L.; Ptacek, C. J.; Blowes, D. W. Zinc isotope fractionation as an indicator of geochemical attenuation processes. *Environ. Sci. Technol. Lett.* **2015**, *2*, 314−319.
(54) Li, W.; Beard, B. L.; Li, C.; Johnson, C. M. Magnesium isotope fractionation between brucite [$Mg(OH)_2$] and Mg aqueous species: Implications for silicate weathering and biogeochemical processes. *Earth Planet. Sci. Lett.* **2014**, *394*, 82−93.

■ NOTE ADDED AFTER ASAP PUBLICATION

This paper was published ASAP on July 31, 2018, with errors in the x-axis in Figure 5. The corrected version was reposted on August 1, 2018.

DOI: 10.1021/acs.est.8b01414
Environ. Sci. Technol. XXXX, XXX, XXX−XXX